progesterone receptors and the absence of human epidermal growth factor receptor 2[47]. Patients with TNBC show resistance to conventional chemotherapies and are in need of effective therapeutic agents to prevent recurrence and improve survival[48]. As shown in Figures 6g and S7, high expression of RPN2 and accumulation of mtp53 were observed in clinical samples of breast cancer tissues associated with lymph node metastasis. Moreover, our results are supported by a recent clinical study that showed that HSP70 expression correlates significantly with metastasis in TNBC patients[49]. Therefore, the concomitant expression of RPN2 and mtp53 could be a novel diagnostic marker for malignant progression and poor prognosis in TNBC. This is currently being investigated in a large cohort of TNBC patients at our NCC hospital and it would reveal that which types of p53 mutants are associated with RPN2 expression.

In summary, the present results indicate that inhibition of the RPN2/mtp53 regulatory network is a promising approach for overcoming the progression of malignant breast tumors and suppressing the CSC phenotype. Furthermore, our data suggest a novel mechanism for the modulation of nucleocytoplasmic proteins in cancer biology. Given the diverse biological roles of RPN2, further investigation aimed at understanding the role of RPN2 in processes associated with tumor progression is warranted.

## Methods

**Plasmids.** N-terminal Flag-tagged Snail (pFlag-Snail), N-terminal Flag-tagged HSF1 (pFlag-HSF1), pBabe-puro-Snail, C-terminal V5-tagged wtp53 (pLenti6/V5-p53), C-terminal V5-tagged mtp53 (R280K, pLenti6/V5-p53R280K) and C-terminal HA-tagged GSK3β (pcDNA3-GSK3β-HA) were purchased from Addgene. To obtain C-terminal Myc- and Flag-tagged RPN2 constructs (pLenti-RPN2-Myc-Flag), cDNA encoding full-length human RPN2 (GenBank accession number Y00282) was amplified by polymerase chain reaction (PCR) using cDNA pools from MDA-MB231-D3H2-LN cells (MM231-LN). PCR fragments were inserted into EcoRI- and NotI-treated pLenti-C-Myc-DDK (Origene: PS100064). To obtain a HSP70 promoter-driven GFP (pHSP70-GFP), HSP70 promoter region was amplified by PCR using genomic DNA from MM231-LN cells (GenBank accession number M11717). The PCR fragment was inserted into BglII- and SalI-treated pEGFP-1 (Clontech). To obtain a HSP70 promoter-driven secreted cypridina luciferase (pHSP70-CLuc), HSP70-GFP was digested with KpnI and NotI and the fragment containing GFP was replaced with cypridina luciferase gene derived from pCLuc-Basic2 (NEB). All constructs were verified by DNA sequencing.

**Cell culture.** MCF7, MCF7-ADR, MCF7-ADR-Luc, MM231-LN, 293T, MCF10A and HME cells have been described previously[14,19]. To establish MM231-LN cells expressing HSP70-GFP, pHSP70-GFP containing the neomycin resistance gene was transfected with lipofectamine LTX (Invitrogen). The transfected cells were cultivated under selective growth medium including G418 (0.6 mg/ml). For spheroid culture, cells were plated on NanoCulture plates (Scivax) and cultured for 3 days.

**Antibodies.** The primary antibodies and dilutions were anti-RPN2 (1 : 2000, sc-166421, Santa Cruz Biotechnology), anti-p53 (1 : 2000, sc-126, Santa Cruz Biotechnology), anti-V5 (1 : 1000, V8137, Sigma), anti-Vimentin (1 : 2000, 550513, BD Pharmingen), anti-HA (1 : 2000, #3724, CST), anti-HSP27(1 : 2000, #2402, CST), anti-Myc (1 : 1000, 2278, CST), anti-Flag (1 : 1000, M185-7, MBL), anti-HA agarose (#3956S, CST), anti-HSP70 (1 : 1000, 610607, BD Transduction Laboratories), anti-HSP90 (1 : 1000, 610418, BD Transduction Laboratories), anti-GSK3β (1 : 1000, 610201, BD Transduction Laboratories), anti-Phospho-GSK3β (Tyr216) (1 : 1000, 612312, BD Transduction Laboratories), anti-N-cadherin (1 : 2000, #4061S, CST) and anti-actin antibodies (1 : 5000, MAB1501, Millipore). An anti-p53 antibody (Abcam, Pab240) was used for the detection of mtp53 by IHC. Staining was visualized using Alexa 488 or Alexa 594 (Molecular Probes). Immunofluorescence-stained cells were observed by fluorescence microscopy or confocal fluorescence microscopy (Leica). The signal intensity in immunoblot analysis was quantified using ImageJ software (http://rsbweb.nih.gov/ij/).

**Lentiviral shRNA transduction.** Cell lines stably expressing *RPN2* shRNA, *14-3-3zeta* shRNA or control non-target shRNA were established using a vector-based shRNA technique. Human *RPN2* shRNA targets 5′-GGAGGAGATTGAGGACCTTGT-3′ (shRPN2-site1), 5′-GCCACTTTGAAGAACCCAATC-3′ (shRPN2-site2), 5′-TCCAGATTGTAGTTATACTTC-3′ (shRPN2-UTR), human *14-3-3zeta* shRNA targets 5′-GCAGAGAGCAAAGTCTTCTAT-3′ (sh14-3-3zeta-site1), 5′-GCAATTACTGAGAGACAACTT-3′ (sh14-3-3zeta-site2), 5′-GCTCGAGAATACAGAGAGAAA-3′ (sh14-3-3zeta-site3), 5′-GAGAGGAATCTTCTCTCAGTT-3′ (sh14-3-3zeta-site4), 5′-CTCTGTGTTCTATTATGAGAT-3′ (sh14-3-3zeta-site5) and control shRNA targets 5′-GAAATGTACTGCGCGTGGAGAC-3′. Briefly, each fragment was subcloned into pGreenPuro (System Biosciences). Recombinant lentiviruses were produced according to the manufacturer's instructions. In knockdown experiments, MCF7-ADR and MM231-LN cells were infected with recombinant lentiviruses expressing control shRNA (shNC) or shRNA against RPN2 (shRPN2).

**Matrigel invasion assay.** The matrigel invasion assay was performed using the Matrigel Invasion Chamber (BD Bioscience) according to the manufacturer's protocol. In brief, $5 \times 10^4$ cells were plated in the upper chamber in serum-free media. The bottom chamber contained RPMI media with 10% FBS. After 24–48 h, the bottom of the chamber insert was fixed and stained with Diff-Quick stain. Cells on the stained membrane were counted under a dissecting microscope. Each membrane was divided into four quadrants and an average from all four quadrants was calculated. The matrigel invasion assays were performed with biological triplicates.

**Dual luciferase assay.** MM231-LN shNC or MM231-LNshRPN2 cells ($2 \times 10^4$ cells) were seeded in a 24-well plate and cotransfected with HSF1 expression vector (pFlag-HSF1) in combination with reporter constructs of HSP70 promoter (pHSP70-Cluc), and SV40 promoter (pSV40-Cluc) using Lipofectamine 2000 (Invitrogen). The amount of plasmid DNA used in each experiment is indicated in the figure legends. A thymidine kinase promoter-driven secreted gaussia luciferase (pTK-Gluc, NEB) was mixed in a DNA–liposome complex as an internal control. Luciferase activity was quantified by a dual-luciferase assay system (NEB) and relative transactivation was calculated according to the manufacturer's instructions. All experiments were repeated at least 3 times.

**Fluorescence-activated cell sorting.** FITC or APC-conjugated anti-CD44 antibody (BD Bioscience, clone G44-26), PE-conjugated anti-CD24 antibody (Biolegend, clone LM5), APC-conjugated anti-E cadherin antibody (Biolegend, clone 67A4) and propidium iodide (5 μg/ml) were used for fluorescence-activated cell sorting (FACS) analysis using JSAN in accordance with the manufacturer's protocols. Data were processed by FlowJo software.

**Immunoprecipitation.** MM231-LN cells were lysed using immunoprecipitation buffer (20 mM Tris–HCl pH 8.0, 150 mM NaCl, 1 mM EDTA, 0.1% NP-40, 10% glycerol, 1 mM DTT, protease inhibitor cocktail, phosphatase inhibitor). After brief sonication, the lysates were cleared by centrifugation at 4°C. Supernatants were incubated with anti-RPN2 or anti- anti-GSK3β antibodies for 4 h and protein A/G-Sepharose beads (Invitrogen) for 4 h at 4°C. The immunocomplexes were washed four times, boiled in sample buffer and immunoblotted with anti-GSK3β, anti-Phospho-GSK3β (Tyr216) and anti-RPN2 antibodies.

**Co-immunoprecipitation analysis.** Extracts of 293T cells were obtained using immunoprecipitation buffer as described above. Supernatants were incubated with anti-HA Agarose (CST) under rotation for 4 h at 4°C. After washing four times with immunoprecipitation buffer, the immunoprecipitated protein complex bound to the beads was eluted with the HA peptide (Wako). The eluates from the immunoprecipitation and cell lysates were immunoblotted with anti-GSK3β, anti-Phospho-GSK3β (Tyr216) and anti-GFP antibodies.

**Real-time reverse transcription PCR.** Total RNA was isolated from cells and tumor tissues with an RNeasy Mini Kit and an RNase-Free DNase Set (Qiagen), and cDNA was produced with an ExScript RT reagent Kit (Takara). The cDNA samples were subjected to real-time PCR with SYBR Premix Ex Taq (Invitrogen) and specific primers (Supplementary Methods). All reactions were performed in a Light Cycler (Applied Biosystems). Gene expression levels were normalized to those of β-actin.

**Bioluminescence imaging.** Animal experiments were performed in compliance with the guidelines of the Institute for Laboratory Animal Research, National Cancer Center Research Institute. Female non-obese diabetic/severe combined immunodeficiency (NOD/SCID) mice (NOD.CB17-Prdkc$^{scid}$/J, CLEA Japan, Shizuoka, Japan) aged 4–6 weeks were anaesthetized by exposure to 3% isoflurane on day zero and subsequent days. Images were analyzed with Living Image software (Xenogen, part of Caliper Life Sciences). Bioluminescent flux (photons$s^{-1}$ $sr^{-1}$ $cm^{-2}$) was determined for the primary tumors, lungs or lymph nodes (upper abdomen, region of interest).

**Mammary fat pad xenografts.** MCF7-ADR or MM231-LN cells were suspended in a PBS/Matrigel (Sigma) mixture (1 : 1) and injected into the mammary fat pad in a 50 μl volume (n = 5 each and $10^2$–$10^6$ cells per animal).

**Tissue arrays.** The tissue arrays of breast cancer samples were purchased from Super Bio CHIP. Immunohistochemical staining of RPN2 and mutant p53 was performed with DAB peroxidase and alkaline phosphatase substrate kits (Vector Laboratories).

**Statistical analysis.** Data are presented as mean ± standard error of the mean (s.e.m.) or mean ± standard deviation (s.d.). Statistical significance was determined by Student's two-tailed *t*-test unless otherwise noted. A $P$ value $< 0.05$ was considered statistically significant.


1. Shaulian, E., Zauberman, A., Ginsberg, D. & Oren, M. Identification of a minimal transforming domain of p53: negative dominance through abrogation of sequence-specific DNA binding. *Mol Cell Biol* **12**, 5581–5592 (1992).
2. Kalo, E. *et al.* Mutant p53 attenuates the SMAD-dependent transforming growth factor beta1 (TGF-beta1) signaling pathway by repressing the expression of TGF-beta receptor type II. *Mol Cell Biol* **27**, 8228–8242 (2007).
3. Muller, P. A. *et al.* Mutant p53 drives invasion by promoting integrin recycling. *Cell* **139**, 1327–1341 (2009).
4. Song, H., Hollstein, M. & Xu, Y. p53 gain-of-function cancer mutants induce genetic instability by inactivating ATM. *Nat Cell Biol* **9**, 573–580 (2007).
5. Adorno, M. *et al.* A Mutant-p53/Smad complex opposes p63 to empower TGFbeta-induced metastasis. *Cell* **137**, 87–98 (2009).
6. Li, D., Marchenko, N. D. & Moll, U. M. SAHA shows preferential cytotoxicity in mutant p53 cancer cells by destabilizing mutant p53 through inhibition of the HDAC6-Hsp90 chaperone axis. *Cell Death Differ* **18**, 1904–1913 (2011).
7. Peng, Y., Chen, L., Li, C., Lu, W. & Chen, J. Inhibition of MDM2 by hsp90 contributes to mutant p53 stabilization. *J Biol Chem* **276**, 40583–40590 (2001).
8. Trepel, J., Mollapour, M., Giaccone, G. & Neckers, L. Targeting the dynamic HSP90 complex in cancer. *Nat Rev Cancer* **10**, 537–549 (2010).
9. Powers, M. V., Clarke, P. A. & Workman, P. Dual targeting of HSC70 and HSP72 inhibits HSP90 function and induces tumor-specific apoptosis. *Cancer Cell* **14**, 250–262 (2008).
10. Yan, W. *et al.* Histone deacetylase inhibitors suppress mutant p53 transcription via histone deacetylase 8. *Oncogene* (2012).
11. Chang, C. J. *et al.* p53 regulates epithelial-mesenchymal transition and stem cell properties through modulating miRNAs. *Nat Cell Biol* **13**, 317–32 (2011).
12. Onder, T. T. *et al.* Loss of E-cadherin promotes metastasis via multiple downstream transcriptional pathways. *Cancer Res* **68**, 3645–3654 (2008).
13. Oft, M., Akhurst, R. J. & Balmain, A. Metastasis is driven by sequential elevation of H-ras and Smad2 levels. *Nat Cell Biol* **4**, 487–494 (2002).
14. Mani, S. A. *et al.* The epithelial-mesenchymal transition generates cells with properties of stem cells. *Cell* **133**, 704–715 (2008).
15. Bachelder, R. E., Yoon, S. O., Franci, C., de Herreros, A. G. & Mercurio, A. M. Glycogen synthase kinase-3 is an endogenous inhibitor of Snail transcription: implications for the epithelial-mesenchymal transition. *J Cell Biol* **168**, 29–33 (2005).
16. Yook, J. I. *et al.* A Wnt-Axin2-GSK3beta cascade regulates Snail1 activity in breast cancer cells. *Nat Cell Biol* **8**, 1398–1406 (2006).
17. Li, Y. *et al.* Sulforaphane, a dietary component of broccoli/broccoli sprouts, inhibits breast cancer stem cells. *Clin Cancer Res* **16**, 2580–2590 (2010).
18. Gupta, P. B. *et al.* Identification of selective inhibitors of cancer stem cells by high-throughput screening. *Cell* **138**, 645–659 (2009).
19. Honma, K. *et al.* RPN2 gene confers docetaxel resistance in breast cancer. *Nat Med* **14**, 939–948 (2008).
20. Clevers, H. The cancer stem cell: premises, promises and challenges. *Nat Med* **17**, 313–319 (2011).
21. Yin, H. & Glass, J. The phenotypic radiation resistance of CD44+/CD24(-or low) breast cancer cells is mediated through the enhanced activation of ATM signaling. *PloS one* **6**, e24080 (2011).
22. Calcagno, A. M. *et al.* Prolonged drug selection of breast cancer cells and enrichment of cancer stem cell characteristics. *Journal of the National Cancer Institute* **102**, 1637–1652 (2010).
23. Al-Hajj, M., Wicha, M. S., Benito-Hernandez, A., Morrison, S. J. & Clarke, M. F. Prospective identification of tumorigenic breast cancer cells. *Proc Natl Acad Sci U S A* **100**, 3983–3988 (2003).
24. Todaro, M. *et al.* Colon cancer stem cells dictate tumor growth and resist cell death by production of interleukin-4. *Cell Stem Cell* **1**, 389–402 (2007).
25. Li, D. *et al.* Functional inactivation of endogenous MDM2 and CHIP by HSP90 causes aberrant stabilization of mutant p53 in human cancer cells. *Mol Cancer Res* **9**, 577–588 (2011).
26. Muller, P., Hrstka, R., Coomber, D., Lane, D. P. & Vojtesek, B. Chaperone-dependent stabilization and degradation of p53 mutants. *Oncogene* **27**, 3371–3383 (2008).
27. Esser, C., Scheffner, M. & Hohfeld, J. The chaperone-associated ubiquitin ligase CHIP is able to target p53 for proteasomal degradation. *J Biol Chem* **280**, 27443–27448 (2005).
28. Zhang, Y. *et al.* HSF1-dependent upregulation of Hsp70 by sulfhydryl-reactive inducers of the KEAP1/NRF2/ARE pathway. *Chem Biol* **18**, 1355–1361 (2011).
29. Chiang, W. C., Ching, T. T., Lee, H. C., Mousigian, C. & Hsu, A. L. HSF-1 regulators DDL-1/2 link insulin-like signaling to heat-shock responses and modulation of longevity. *Cell* **148**, 322–334 (2012).
30. Xavier, I. J. *et al.* Glycogen synthase kinase 3beta negatively regulates both DNA-binding and transcriptional activities of heat shock factor 1. *J Biol Chem* **275**, 29147–29152 (2000).
31. Kim, D., Kim, S. H. & Li, G. C. Proteasome inhibitors MG132 and lactacystin hyperphosphorylate HSF1 and induce hsp70 and hsp27 expression. *Biochem Biophys Res Commun* **254**, 264–268 (1999).
32. Liu, J. *et al.* p27 suppresses arsenite-induced Hsp27/Hsp70 expression through inhibiting JNK2/c-Jun- and HSF-1-dependent pathways. *J Biol Chem* **285**, 26058–26065 (2010).
33. Wei, L. *et al.* Hsp27 participates in the maintenance of breast cancer stem cells through regulation of epithelial-mesenchymal transition and nuclear factor-kappaB. *Breast Cancer Res* **13** (2011).
34. Ogretmen, B. & Safa, A. R. Expression of the mutated p53 tumor suppressor protein and its molecular and biochemical characterization in multidrug resistant MCF-7/Adr human breast cancer cells. *Oncogene* **14**, 499–506 (1997).
35. Ono, M. *et al.* Prolyl 4-hydroxylation of alpha-fibrinogen: a novel protein modification revealed by plasma proteomics. *J Biol Chem* **284**, 29041–29049 (2009).
36. Neal, C. L. & Yu, D. 14-3-3zeta as a prognostic marker and therapeutic target for cancer. *Expert Opin Ther Targets* **14**, 1343–1354 (2010).
37. Danes, C. G. *et al.* 14-3-3 zeta down-regulates p53 in mammary epithelial cells and confers luminal filling. *Cancer Res* **68**, 1760–1767 (2008).
38. Zambetti, G. P. & Levine, A. J. A comparison of the biological activities of wild-type and mutant p53. *FASEB J* **7**, 855–865 (1993).
39. Cohen, P. & Frame, S. The renaissance of GSK3. *Nat Rev Mol Cell Biol* **2**, 769–776 (2001).
40. Crimaudo, C., Hortsch, M., Gausepohl, H. & Meyer, D. I. Human ribophorins I and II: the primary structure and membrane topology of two highly conserved rough endoplasmic reticulum-specific glycoproteins. *EMBO J* **6**, 75–82 (1987).
41. Wilson, C. M., Roebuck, Q. & High, S. Ribophorin I regulates substrate delivery to the oligosaccharyltransferase core. *Proc Natl Acad Sci U S A* **105**, 9534–9539 (2008).
42. Ge, X., Loh, H. H. & Law, P. Y. mu-Opioid receptor cell surface expression is regulated by its direct interaction with Ribophorin I. *Mol Pharmacol* **75**, 1307–1316 (2009).
43. Mehta, P. P. *et al.* Effective targeting of triple-negative breast cancer cells by PF-4942847, a novel oral inhibitor of Hsp 90. *Clin Cancer Res* **17**, 5432–5442 (2011).
44. Yiu, C. C. *et al.* Down-regulation of heat-shock protein 70 (HSP-70) correlated with responsiveness to neoadjuvant aromatase inhibitor therapy in breast cancer patients. *Anticancer Res* **30**, 3465–3472 (2010).
45. Li, Y. *et al.* Amplification of LAPTM4B and YWHAZ contributes to chemotherapy resistance and recurrence of breast cancer. *Nat Med* **16**, 214–218 (2010).
46. Bug, M. & Dobbelstein, M. Anthracyclines induce the accumulation of mutant p53 through E2F1-dependent and -independent mechanisms. *Oncogene* (2011).
47. Cleator, S., Heller, W. & Coombes, R. C. Triple-negative breast cancer: therapeutic options. *Lancet Oncol* **8**, 235–244 (2007).
48. Gluz, O. *et al.* Triple-negative breast cancer--current status and future directions. *Ann Oncol* **20**, 1913–1927 (2009).
49. Sun, B. *et al.* Identification of metastasis-related proteins and their clinical relevance to triple-negative human breast cancer. *Clin Cancer Res* **14**, 7050–7059 (2008).


## Acknowledgments

We thank Dr S. Koizumi for providing the human mammary carcinoma cell lines MCF7, MCF7-ADR and MDA-MB-231-D3H2-LN, Dr Y. Yamamoto for helpful discussions and Miss. A. Inoue for her excellent technical assistance. This study was supported in part by a grant-in-aid for the Third-Term Comprehensive 10-Year Strategy for Cancer Control of Japan, a grant-in-aid for Scientific Research on Priority Areas Cancer from the Japanese Ministry of Education, Culture, Sports, Science and Technology, and the Program for Promotion of Fundamental Studies in Health Sciences of the National Institute of Biomedical Innovation of Japan, and supported by a Funding Program for World-Leading Innovative R&D on Science and Technology (FIRST Program) from the Japan Society for the Promotion of Science (JSPS).

## Author contributions

R.T. and K.H. designed the experiments and analysed the data. R.T. and F.T. performed the experiments. K.K. provided human breast cancer pathology information. M.O. performed proteome analysis by 2DICAL. R.T. and T.O. wrote the manuscript. All authors discussed the results and commented on the manuscript.

## Additional information

**Supplementary information** accompanies this paper at http://www.nature.com/scientificreports

**Competing financial interests:** The authors declare no competing financial interests.

**How to cite this article:** Takahashi, R.-u. *et al.* Ribophorin-2 regulates breast tumor initiation and metastasis through the functional suppression of GSK3β. *Sci. Rep.* 3, 2474; DOI:10.1038/srep02474 (2013).

⌘ *Author's Choice*

THE JOURNAL OF BIOLOGICAL CHEMISTRY VOL. 288, NO. 15, pp. 10849–10859, April 12, 2013


# Neutral Sphingomyelinase 2 (nSMase2)-dependent Exosomal Transfer of Angiogenic MicroRNAs Regulate Cancer Cell Metastasis*[S]

Received for publication, December 18, 2012, and in revised form, February 18, 2013 Published, JBC Papers in Press, February 25, 2013, DOI 10.1074/jbc.M112.446831

**Nobuyoshi Kosaka[‡], Haruhisa Iguchi[‡§], Keitaro Hagiwara[‡¶], Yusuke Yoshioka[‡1], Fumitaka Takeshita[‡], and Takahiro Ochiya[‡2]**

*From the [‡]Division of Molecular and Cellular Medicine, National Cancer Center Research Institute, 5-1-1, Tsukiji, Chuo-ku, Tokyo 104-0045, Japan, the [§]Pharmacology Research Laboratories, Dainippon Sumitomo Pharma Co., Ltd., 1-98 Kasugadenaka 3-chome, Konohana-ku, Osaka 554-0022, Japan, and the [¶]Department of Biological Information, Graduate School of Bioscience and Biotechnology, Tokyo Institute of Technology, Yokohama, Kanagawa 226-8501, Japan*

**Background:** Contribution of exosomal microRNAs to cancer metastasis remains unknown.
**Results:** Exosomal angiogenic microRNAs secreted by metastatic cancer cells promote the metastasis through the activation of endothelial cells.
**Conclusion:** Horizontal transfer of exosomal miRNAs from cancer cells can dictate the microenviromental niche for the benefit of the cancer cell.
**Significance:** This is the first to connect cancer metastasis to the exosomal microRNA *in vivo*.

**The release of humoral factors between cancer cells and the microenvironmental cells is critical for metastasis; however, the roles of secreted miRNAs in non-cell autonomous cancer progression against microenvironmental cells remain largely unknown. Here, we demonstrate that the neutral sphyngomyelinase 2 (nSMase2) regulates exosomal microRNA (miRNA) secretion and promotes angiogenesis within the tumor microenvironment as well as metastasis. We demonstrate a requirement for nSMase2-mediated cancer cell exosomal miRNAs in the regulation of metastasis through the induction of angiogenesis in inoculated tumors. In addition, miR-210, released by metastatic cancer cells, was shown to transport to endothelial cells and suppress the expression of specific target genes, which resulted in enhanced angiogenesis. These findings suggest that the horizontal transfer of exosomal miRNAs from cancer cells can dictate the microenviromental niche for the benefit of the cancer cell, like "on demand system" for cancer cells.**

The secretion of humoral factors from cancer cells to microenvironmental cells is essential for metastasis during cancer development (1). Although microRNAs (miRNAs)[3] are known as tumor suppressors of cell autonomous malignancy phenotypes such as metastasis (2) and multidrug resistancy (3), the roles of miRNAs in non-cell autonomous cancer progression against microenvironmental cells remain largely unknown. The existence of secretory RNA has been known for many years (4, 5), and recent reports have shown that miRNAs (6), which regulate various types of biological phenomena through the regulation of a variety of target genes, are secreted from cells via the exosome (7, 8). These findings have raised the possibility that RNAs, including miRNAs, may serve as novel humoral factors in cell-cell communication (9). We recently demonstrated that miRNAs are released through neutral sphingomyelinase 2 (nSMase2)-regulated secretory machinery and that these secretory miRNAs are transferable and functional in recipient cells (10). Furthermore, we also found that a tumor-suppressive miRNA secreted from non-cancerous cells via this pathway could be transported between cells and exert gene silencing in the recipient cancer cells, thereby leading to an inhibition of cancer cell growth (11). In the last few years, it has become clear that exosomal miRNAs play critical roles in mediating cell-cell communication, specifically between immune cells, endothelial cells and cancer cells (12–17). These findings provide evidence that exosomal miRNAs are required for cell-cell communication in various physiological and pathological conditions, although the contribution of extracellular miRNAs to cancer metastasis remains largely unknown (9). Here, we first demonstrated that horizontal transfer of exosomal miR-210 from metastatic cancer cells could dictate the microenvironmental endothelial cells to the benefit of the cancer cells, which contributed to cancer metastasis. Preventing the expression of

* This work was supported in part by a grant-in-aid for the third term comprehensive 10-year strategy for cancer control, a grant-in-aid for scientific research on priority areas cancer from the Ministry of Education, Culture, Sports, Science, and Technology, and the Program for Promotion of Fundamental Studies in Health Sciences of the National Institute of Biomedical Innovation (NiBio), and the Japan Society for the Promotion of Science through the Funding Program for world leading innovative R&D on science and technology (FIRST Program) initiated by the Council for Science and Technology Policy, and a grant-in-aid for Scientific Research on Innovative Areas (functional machinery for non-coding RNAs) from the Japanese Ministry of Education, Culture, Sports, Science, and Technology.
⌘ *Author's Choice*—Final version full access.
[S] This article contains supplemental Figs. 1–9.
[1] A research fellow for the Japan Society for the Promotion of Science.
[2] To whom correspondence should be addressed: Div. of Molecular and Cellular Medicine, National Cancer Center Research Inst., 1-1 Tsukiji, 5-chome, Chuo-ku, Tokyo 104-0045, Japan. Tel.: 81-3-3542-2511 (ext. 4800); Fax: 81-3-5565-0727; E-mail: tochiya@ncc.go.jp.

[3] The abbreviations used are: miRNA, microRNA; nSMase2, neutral sphingomyelinase 2; KD, knockdown; luc, luciferase; HUVEC, human umbilical cord vein endothelial cell; nSMase2-OE, nSMase2-overexpressing cancer cells; qRT-PCR, quantitative RT-PCR.

nSMase2 in metastatic cancer cells abrogates the metastatic ability of cancer cells to target lung tissues, whereas reconstitution via the administration of exosomes isolated from metastatic cancer cells rescued this phenomenon. In this context, the number of endothelial cells in inoculated tumors was proportional to the expression level of nSMase2 in cancer cells. In fact, exosomes derived from a metastatic cancer cell line enhanced the capillary formation and migration of endothelial cells *in vitro*. Interestingly, the expression profiles of exosomal miRNAs obtained from metastatic cancer cells demonstrated that a set of angiogenic miRNAs were highly concentrated in these exosomes. One of them, miR-210, enhanced the angiogenesis through the suppression of specific target gene, which resulted in enhanced angiogenesis. These results revealed that cancer cells provide nSMase2-regulated exosomal miRNAs to endothelial cells to promote their metastatic initiation efficiency.

## EXPERIMENTAL PROCEDURES

*Reagents*—Goat polyclonal anti-Alix (Q-19; sc-49268) and donkey anti-goat IgG (HRP; sc-2020) were purchased from Santa Cruz Biotechnology. Mouse monoclonal anti-HSP70, clone 7/HSP70 (610607), and mouse monoclonal ant-human CD63 antibody (556019) were purchased from BD Biosciences. Rabbit polyclonal anti-CD31 antibody (ab28364) was from Abcam. Peroxidase-labeled anti-mouse antibodies were purchased from GE Healthcare (NA931V). GW4869 was purchased from Calbiochem (Darmstadt, Germany). Geneticin and puromycin were purchased from Invitrogen.

*Cell Culture*—4T1 cells, a mouse breast cancer cell line, MCF7, non-metastatic breast cancer cells, and MCF10A, normal mammary epithelial cells, were obtained from the American Type Culture Collection (Manassas, VA). MDA-MB-231-D3H1 and MDA-MB-231-D3H2LN, a metastatic human breast cancer cell line, were obtained from Xenogen. 4T1, MCF7, MDA-MB-231-D3H1, and MDA-MB-231-D3H2LN were cultured in RPMI containing 10% heat-inactivated FBS and antibiotic-antimycotic (Invitrogen) at 37 °C in 5% $CO_2$. Human umbilical cord vein endothelial cells (HUVECs) were purchased from Lonza and cultured in EBM-2 BulletKit (Lonza) supplemented with 2% FBS.

*Exosome Purification*—Exosomes were purified by differential centrifugation as described previously (10). The exosome fraction was measured for its protein content using the Micro BCA protein assay kit (Thermo Scientific, Wilmington, DE).

*Tube Formation Assay*—HUVECs (100,000) cells were cultured on 150 μl of Matrigel (Sigma) in culture medium for 16 h in 24-well plate. The degree of tube formation was quantified by measuring the number of branches in five randomly chosen fields from each well using NIH ImageJ software. For rescue experiments, HUVECs were transfected using Dharmafect reagent (Dharmacon) according to the manufacturer's recommendations with anti-control or anti-miR-210 (Ambion). After 24 h of posttransfection, cells were seeded onto Matrigel as described above with 1 μg of exosome.

*Establishment of Stable Cell Lines*—A stable 4T1 and MDA-MB-231-D3H2LN nSMase2-modified cell lines that expressed mouse nSMase2 shRNA, human nSMase2 shRNA, and pCT-CD63-GFP were generated by selection with puromycin. A stable 4T1 and MDA-MB-231-D3H2LN cell lines that overexpresses human nSMase2 were generated by selection with geneticin. 4T1 cells or MDA-MB-231-D3H2LN were transfected with 0.5 μg of the vector at 90% confluency in 24-well dishes using a Lipofectamine LTX reagent in accordance with the manufacturer's instructions.

*Co-culture Experiments*—Well inserts for 24-well plates with a 0.4-μm pore-sized filter were purchased from BD and used following the manufacturer's instructions. 4T1 control cells, 4T1-nSMase2-KD cells, 4T1-siLuc cells, or 4T1-CD63-GFP cells (100, 000) were seeded into the well inserts. HUVECs (200, 000) were seeded into 24-well plates.

*Confocal Microscopy*—Confocal microscopy was done on an Olympus laser scanning microscope FV10i (Olympus). Filters used were 489–510 nm (GFP and Alexa Fluor 488) and 577–603 nm (Alexa Fluor 568).

*Immunoblot Analysis*—Exosomes were lysed in a 2% SDS buffer, and equal amounts of protein were loaded onto an SDS-PAGE gel. Anti-Alix (1:200), anti-HSP70 (1:1,000), and anti-CD63 (1:200) were used as primary antibodies. The dilution ratio of each antibody is indicated in *parentheses*. Two secondary antibodies (peroxidase-labeled anti-goat and anti-mouse antibodies) were used at a dilution of 1:2000. Bound antibodies were visualized by chemiluminescence using the ImmunoStar LD (290-69904) (Wako), and luminescent images were analyzed by a LuminoImager (LAS-3000; Fujifilm, Inc.). Only gels for CD63 (BD Biosciences) detection were run under non-reducing conditions.

*Plasmids*—psiRNA-LucGL3 was purchased from InvivoGen. Knockdown shRNA vector for human and mouse nSMase2 were purchased from TaKaRa Bio. A full-length human nSMase2 cDNA was cloned into pIRES2-EGFP vector (Clontech). Primary miR-210 were PCR-amplified from human genomic DNA and cloned into the downstream of CMV promoter in pIREShyg3 (Takara Bio). The sensor vector for miR-210 was constructed by introducing tandem binding sites with perfect complementarity to miR-210, separated by a four-nucleotide spacer into the XhoI site of psiCHECK2 (Promega). The sequences of the binding site are as follows: 5′-TTCTCGAGTTTCAGCCG-CTGTCACACGCACAGTTACGCGTTTTCAGCCGCTGT-CACACGCACAGTTCTCGAGTT-3′ (sense) and 5′-AACTC-GAGAACTGTGCGTGTGACAGCGGCTGAAAACGCGT-AACTGTGCGTGTGACAGCGGCTGAAACTCGAGAA-3′ (antisense). The "seed" sequence of miR-210 is *underlined*. In a mutated miR-210 sensor vector, the seed sequence, ACACGCA, was displaced with TGTGCGT. All of the plasmids were verified by DNA sequencing.

*Isolation of RNAs*—Isolation of exosomal and cellular RNAs was performed using the miRNeasy Mini Kit (Qiagen). Exosome or cell lysate was diluted with 1 ml of Qiazol solution. Subsequent extraction and filter cartridge work were carried out according to the manufacturer's protocol.

*mRNA and miRNA Expression Analysis*—The method for qRT-PCR has been described previously (10). PCR was carried out in 96-well plates using the 7300 Real Time PCR system (Applied Biosystems). All reactions were done in triplicate. All TaqMan MicroRNA assays were purchased from Applied Bio-

systems. RNU6 was used as an invariant control for the cells. Gene expression was analyzed using Taqman gene expression assays except primary miR-210 (Applied Biosystems). The expression levels of primary miR-210 and β-actin were measured by qRT-PCR using a SYBR Green PCR Master Mix (Invitrogen). Primer sequences are as follows (shown 5′ to 3′): primary miRNA-210, GACTGGCCTTTGGAAGCTCC (forward) and ACAGCCTTTCTCAGGTGCAG (reverse); β-actin, GGCACCACCATGTACCCTG (forward) and CACGGAGTACTTGCGCTCAG (reverse).

*Nanoparticle Tracking Analysis*—Nanoparticle tracking analysis was carried out using the Nanosight LM10-HS system (NanoSight) on exosomes resuspended in PBS and were further diluted for analysis. The results are presented as the average ± S.E. of three independent experiments.

*Phase Contrast Electron Microscopy*—A drop of the sample was put on a copper grid and coated with a carbon film with holes in it. Most of the liquid was removed with blotting paper, leaving a thin film stretched over the holes. The specimen was instantly shock-frozen by plunging into liquid ethane, which was cooled to 90 K by liquid nitrogen into a temperature-controlled freezing unit (Zeiss, Oberkochen, Germany). The remaining ethane was removed with blotting paper, and the specimen was transferred to the electron microscope. The phase plate was prepared from amorphous carbon films. The films were deposited by vacuum evaporation (JEOL JEE-400) on a freshly cleaved mica surface. For observation at 300-kV acceleration voltage, the film thickness corresponding to the *p*/two-phase plate was approximately 32 nm. At that thickness, the transparency of 300-kV acceleration electrons was estimated to be 70%. After preparation, the films were floated on the water's surface and then transferred to a molybdenum aperture with several holes 50-lm in diameter, which resulted in a cut-off frequency for special resolution of 0.5 nm. A hole approximately 0.5 lm in diameter in the center of the carbon film was used by a focused ion beam machine (JEOL JFIB-2000).

*PKH67-labeled Exosome Transfer*—Purified exosomes derived from 4T1 conditioned medium were labeled with a PKH67 green fluorescent labeling kit (Sigma-Aldrich). Exosomes were incubated with 2 μM PKH67 for 5 min, washed four times using 100-kDa filter (Microcon YM-100, Millipore) to remove excess dye, and incubated with HUVECs at 37 °C.

*Microarray Analysis*—To detect the miRNAs in exosomes and cells derived from HEK293, MCF10A, MCF7, and MDA-MB-231, 100 ng of total RNA was labeled and hybridized using a human microRNA microarray kit (Agilent Technologies) according to the manufacturer's protocol (protocol for use with Agilent MicroRNA microarrays, version 1.5). Hybridization signals were detected using a DNA microarray scanner (Agilent Technologies), and the scanned images were analyzed using Agilent Feature Extraction software.

*Mouse Studies*—Animal experiments in this study were performed in compliance with the guidelines of the Institute for Laboratory Animal Research, National Cancer Center Research Institute. Five- to seven-week-old female Balb/c athymic nude mice (CLEA Japan, Shizuoka, Japan) or SCID Hairless Outbred mice (Charles River Laboratories, Kanagawa, Japan) were anesthetized by exposure to 3% isoflurane for injections and *in vivo* imaging. We injected 4T1- or MDA-MB-231-D3H2LN-nSMase2-modified cells bilaterally into the subcutaneous ($2 \times 10^6$ cells were injected in 100-μl volume PBS) or mammary fat pad ($2 \times 10^6$ cells were injected in 50-μl volume Matrigel diluted with PBS) of anesthetized mice. We monitored mammary tumor growth by regular measurements using a digital caliper. After 3 to 4 weeks, we killed mice and determined metastasis in lungs by *ex vivo* or *in vivo* imaging. We carried out lung colonization assays by injecting $1 \times 10^6$ 4T1-control or 4T1-nSMase2-KD cells (suspended in 100 μl of PBS) into the lateral tail vein. Lung colonization was studied and determined by *in vivo* luminescence imaging. For rescue experiment, 4T1-nSMase2-KD cells ($2 \times 10^6$ cells suspended in 100 μl of PBS) were subcutaneously injected. After 4 days of implantation, 1 μg of exosome was injected intratumoraly (100 μl in PBS) every other day for up to 18 days. Metastasis occurrence was determined by *in vivo* luminescence. For *in vivo* imaging, the mice were administered D-luciferin (150 mg/kg, Promega) by intraperitoneal injection. Ten minutes later, photons from animal whole bodies were counted using the IVIS imaging system (Xenogen) according to the manufacturer's instructions. Data were analyzed using LIVINGIMAGE software (version 2.50, Xenogen).

*Statistics*—Statistical analyses were performed using the Student's *t* test.

## RESULTS

*nSMase2 Regulates Cancer Cell Metastasis*—In a previous study, we have described how miRNAs are released through ceramide-dependent secretory machinery via the exosome (10). Specifically, we demonstrated that blocking the activity of nSMase2 resulted in reduced miRNA secretion and that nSMase2 overexpression led to increased levels of extracellular miRNAs (10, 11). In addition, we found that the expression level of nSMase2 was higher in cancer cells than that in non-cancer cells (Fig. 1*A*, *upper panel* and supplemental Fig. 1*A*). Furthermore, secretion level of exosome show correlation with the expression level of nSMase2 (Fig. 1*A*, *lower panel*, and supplemental Fig. 1*B*), suggesting that malignant cancer cells secrete more exosomes than non-cancer cells through the regulation of nSMase2. We confirmed that breast cancer cells secreted around 100-nm size of vesicles with a consistent size and uniform expression of known exosome marker, CD63 and HP70 (supplemental Fig. 1*C*) (18). Purified exosomes has also been shown by phase contrast electron microscopy and found that their size observed to be 90 ± 11.7 nm in diameter ($n = 13$) (Fig. 1*B*). To determine the role of nSMase2 in cancer cell malignancy, we employed 4T1 cells, which are mouse mammary tumor cells with a high tumorigenic and metastatic ability. Both stable nSMase2-knockdown and nSMase2-overexpressing 4T1 cells were generated (supplemental Figs. 1, *D* and *E*) and inoculated into mammary fat pad of the mice, and the tumors were subsequently evaluated for their metastatic colonization capacity in lung tissue. The expression of secretory miR-16 (supplemental Fig. 2*A*), which is known to abundantly existed in exosome, as well as exosome quantity, as determined by immunoblotting for exosome markers, HSP70 and Alix (supplemental Fig. 2*B*), protein concentration (supplemental Fig. 2*C*), and nanopar-

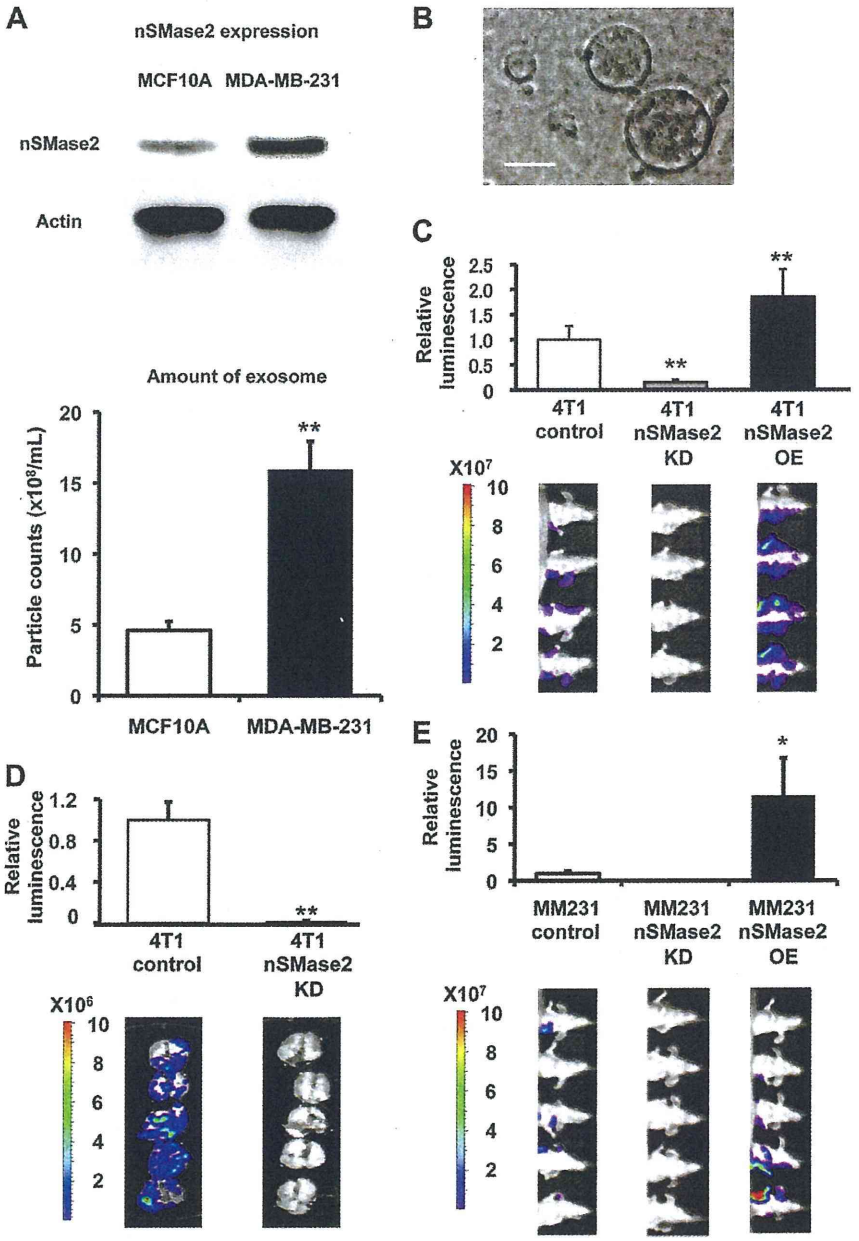


FIGURE 1. **nSMase2 regulates cancer cell metastasis.** *A*, the expression level of nSMase2 protein in (*upper panel*) and secretion level of exosome from (*lower panel*) MCF10A and MDA-MB-231 cells. The same number of cells was seeded. *Error bars* are presented as the mean S.E. ($n = 3$). **, $p < 0.005$, as compared with MCF10A cells. *B*, phase-contrast electron microscopy was used to image resuspend exosome pellets. *Scale bar*, 100 nm. *C*, bioluminescence quantification of lung metastasis by 4T1-control cells, 4T1-nSMase2-KD cells or 4T1-nSMase2-OE cells. Each *error bar* is presented as the mean S.E. ($n = 4$). **, $p < 0.005$, as compared with 4T1-control cells. *D*, luciferase activity in the lung, which was used to represent lung metastasis, was recorded for each mouse. Lung images from different mice are shown. Each *error bar* is presented as the mean S.E. ($n = 5$). **, $p < 0.005$, as compared with 4T1-control cells. *E*, bioluminescence quantification of metastasis by parental MDA-MB-231-D3H2LN (*MM231-control*) cells, MDA-MB-231-D3H2LN-nSMase2-OE (*MM231-nSMase2-OE*) cells, or MDA-MB-231-D3H2LN-nSMase2-KD (*MM231-nSMase2-KD*) cells. Each *error bar* is presented as the mean ± S.E. ($n = 5$). *, $p < 0.05$, as compared with MM231-control cells.

ticle tracking analysis (supplemental Fig. 2*D*), decreased in nSMase2-knockdown cancer cells (4T1-nSMase2-KD cells) but increased in nSMase2-overexpressing cancer cells (4T1-nSMase2-OE cells). However, the expression of intracellular miRNAs was not altered in either of these established cell types (supplemental Figs. 2*A* and 3). After the orthotopic inoculation of these cell lines into mammary fat pad, we found that nSMase2 silencing in parental 4T1 breast cancer cells significantly decreased lung metastatic colonization (Fig. 1*C*), and *in vivo* imaging and histological observation revealed a significant decrease in the total number of metastatic nodules in nSMase2-knockdown lung tumors (Fig. 1*D* and supplemental Fig. 4*A*). In contrast, the overexpression of nSMase2 in 4T1 cells enhanced the metastatic capacity of these tumors (Fig. 1*C*). We also confirmed similar results using an orthotopic model of MDA-MB-231-D3H2LN cells, which are human breast cancer cells with a

high metastatic ability, overexpressing or inhibiting nSMase2 (Fig. 1*E*), which suggests that the alteration in expression level of nSMase2 leads to the change in metastatic ability of cancer cells. Interestingly, nSMase2 inhibition or overexpression in 4T1 cells did not significantly enhance or inhibit cellular proliferation, invasion, or migration *in vitro* (supplemental Fig. 4*B*) and did not increase the mammary tumor volume (supplemental Fig. 4, *C* and *D*). In addition, no significant differences were found in expression profiles of cellular or miRNAs isolated from these nSMase2-modified cell lines (supplemental Fig. 3). Moreover, no significant reduction in metastatic potential was observed in the lungs of animals intravenously injected with parental 4T1 cells or 4T1-nSMase2-KD cells, which excludes the possibility that nSMase2 disruption affected the recruitment capacity of cancer cells to metastatic tissues (supplemental Fig. 5). These results indicate that the effect of nSMase2 on metastasis was not simply due to its effect on the cancer cells themselves.

*Endothelial Activation Regulated by nSMase2-mediated Exosome Promotes Cancer Cell Metastasis*—Consistent with a role for nSMase2 in the initiation of metastasis, intratumor injection of exosomes isolated from parental 4T1 cells to non-metastatic 4T1-nSMase2-KD cells after orthotopical inoculation into mammary fat pad significantly enhanced their metastatic colonization (Fig. 2*A* and supplemental Fig. 6*A*), whereas the growth of the inoculated 4T1-nSMase2-KD tumor cells was unaffected (supplemental Fig. 6*B*). These results indicated that endogenous nSMase2 could act to enhance metastatic initiation through the secretion of exosomes. When examining the selective disadvantage provided by nSMase2 silencing in cancer cells, we noticed that blood vessels were difficult to detect in animals that received 4T1-nSMase2-KD cells (Fig. 2*B*, *left panel*). As a result, we hypothesized that tumors inoculated with nSMase2-knockdown cells would display reduced blood vessel densities upon microscopic visualization of the primary tumor after staining for the endothelial marker CD31. The imaging analysis revealed that primary tumors derived from 4T1-nSMase2-KD cells had significantly lower endothelial cell densities than did tumors derived from control cells (Fig. 2*B*, *right panel*, and 2*C*). In contrast, tumors derived from 4T1-nSMase2-OE cells displayed higher endothelial densities than did tumors derived from control cells (Fig. 2*B*, *right panel*, and 2*C*). In addition, there were increased numbers of endothelial cells in tumors derived from 4T1-nSMase2-KD cells that were subsequently injected with parental 4T1 cell-derived exosomes compared with control treatment (Fig. 2, *D* and *E*). Thus, these observations indicate that release of nSMase2-mediated exosome enhances endothelial cell density, whereas the inhibition of nSMase2 provides metastatic cells with a selective disadvantage for endothelial interactions and angiogenic progression.

*Exosomes Derived from Metastatic Cancer Cells Enhances Activity of Endothelial Cells*—We next sought to determine the cellular basis for nSMase2-regulated exosome-dependent angiogenesis. For this purpose, we first evaluated the effect of exosome from parental 4T1 cells in HUVECs. As a result, although cellular proliferation of HUVECs was slightly increased by the addition of 4T1 exosome (supplemental Fig. 7*A*), addition of purified exosomes derived from metastatic 4T1 cells enhanced not only tube formation in HUVECs, as assessed by the quantification of branch points (Fig. 3*A*), but also migration of HUVECs (Fig. 3*B*). Next, to determine whether exosomes secreted by metastatic breast cancer cells could be incorporated in a paracrine manner, we employed a co-culture system for HUVECs and 4T1 cells, in which the cells are separated by a membrane with a 0.4-$\mu$m pore size to prevent direct cell contact or the transfer of larger vesicles. In this experiment, we used 4T1 cells that had been transduced with a CD63-GFP fusion gene, and we analyzed GFP fluorescence present in HUVECs after 3 days of co-culture by confocal microscopy. These studies showed that exosomes could be transferred from breast cancer cells to endothelial cells during co-culture (Fig. 3*C*, *left panel*). However, the transfer of exosomes from cancer cells to endothelial cells was completely abolished by the addition of nSMase2 inhibitor, GW4869 that was reported to inhibit the secretion of exosome from cells (10, 19), to the 4T1-CD63-GFP cells (Fig. 3*C*: right panel). In addition, 4T1 exosomes labeled with the fluorescent dye PKH67 were cultured with HUVECs and were found to be internalized into endosome-like structures by endothelial cells (supplemental Fig. 7*B*). To confirm whether the exosomes from inoculated cancer cells were incorporated into endothelial cells *in vivo*, an immunohistochemical analysis was performed following the inoculation of 4T1-hCD63 cells *in vivo* (Fig. 3*D*). As shown in Fig. 3*D*, the CD31-positive cells (*green*) was co-localized with CD63 (*red*) signals in the tumor. These findings reveal that enhanced tube formation in endothelial cells is a key feature of metastatic breast cancer cell populations that is regulated in a humoral fashion by exosomes released from metastatic cancer cells.

*Exosomal Angiogenic miRNAs from Cancer Cells Regulate Angiogenesis in Endothelial Cells*—It is well known that angiogenic miRNAs regulate multiple endothelial cell functions and that nSMase2 is essential for miRNA secretion from cells (10, 20, 21). These reports, in addition to our findings described above, prompted us to evaluate the hypothesis that exosomal miRNAs from cancer cells are responsible for this phenomenon. To prove this hypothesis, we used 4T1 cells that had been transduced with a luciferase short hairpin RNA-overexpressing vector (4T1-siLuc). This established cell line secretes luciferase siRNA molecules with a nucleic acid sequence not present in the mammalian genome (supplemental Fig. 8*A*). To evaluate whether the transfer of luciferase siRNA occurred in the form of exosome transfer, we added GW4869 to co-cultured 4T1-siLuc cells and assessed the transfer of luciferase siRNA to HUVECs by qRT-PCR. Although we were able to measure luciferase siRNA in control-treated HUVECs, this siRNA sequence was minimally detected in HUVECs co-cultured with GW4869 treated 4T1-siLuc cells (Fig. 4*A*), which indicates that small RNAs, including not only siRNA but also miRNA, could in fact be transferred from cancer cells to endothelial cells during co-culture and that the transfer of small RNAs is mediated by exosome release regulated by nSMase2. We next sought to determine whether exosomal miRNAs could selectively regulate the angiogenesis of endothelial cells. To address this hypothesis, we performed a miRNA microarray analysis of the following four cell lines: metastatic breast cancer cells (MDA-MB-231); non-metastatic cancer cells (MCF7); normal mam-

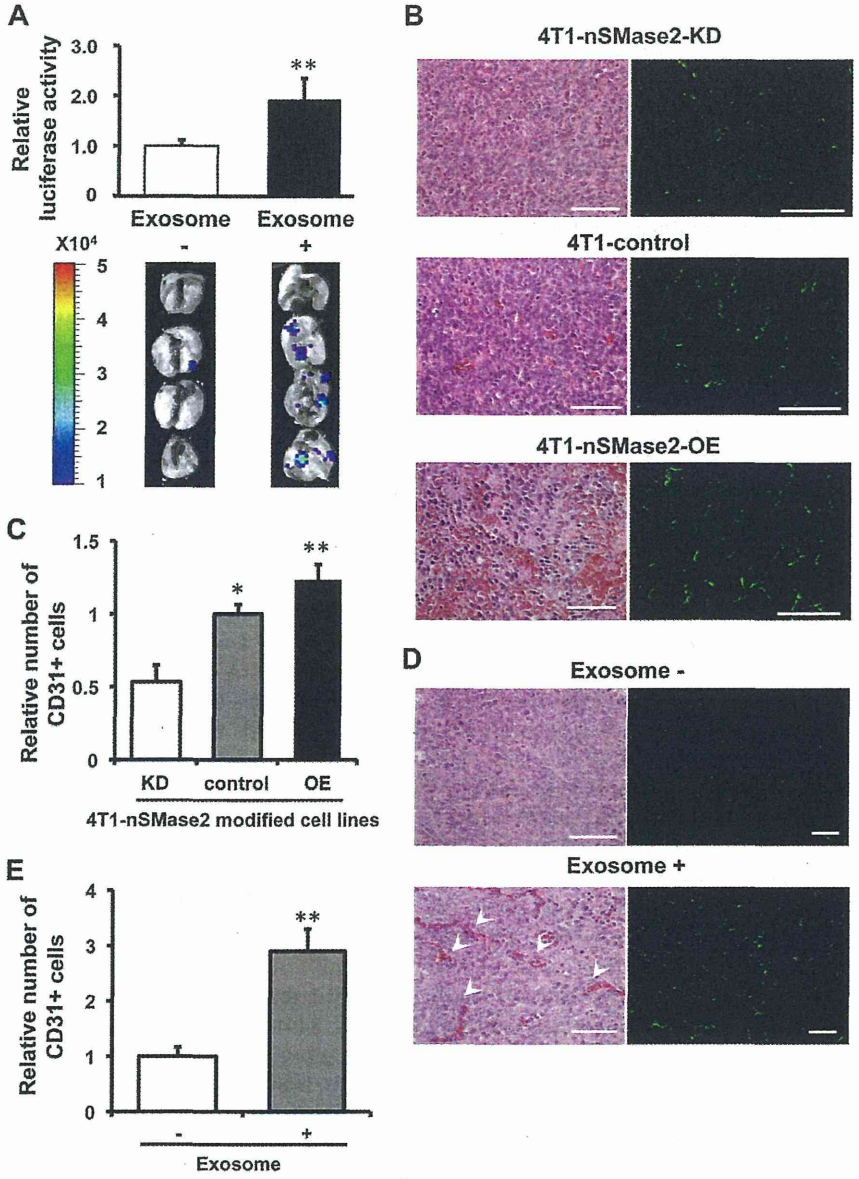


FIGURE 2. **Endothelial activation mediated by nSMase2 regulates cancer cell metastasis.** *A*, bioluminescence imaging of lung metastasis by 4T1-nSMase2-KD cells with or without the injection of exosomes isolated from parental 4T1 cells. Each *error bar* is presented as the mean ± S.E. ($n = 4$). **, $p < 0.005$, as compared with control injection. *B*, H&E of primary tumors isolated from parental 4T1-control cells, 4T1-nSMase2-KD cells or 4T1-nSMase2-OE cells (*left panel*). *Scale bars*, 100 μm for H&E. The endothelial cells were also evaluated using CD31 staining to detect blood vessels in tumors composed of parental 4T1 cells, 4T1-nSMase2-KD cells or 4T1-nSMase2-OE cells (*right panel*); *scale bars*, 100 μm. *C*, angiogenesis determined using CD31 staining which shown in *B* to detect blood vessels in tumors composed of parental 4T1 cells, 4T1-nSMase2-KD cells, or 4T1-nSMase2-OE cells, as above; $n = 4$ for each group. Each *error bar* is presented as the mean ± S.E. ($n = 4$). *, $p < 0.05$; **, $p < 0.005$, as compared with 4T1 control. *D*, H&E staining of primary tumors isolated from mice that received PBS or an injection of exosomes from parental 4T1 cells following the transplantation of 4T1-nSMase2-KD cells (*left panel*). *Arrowheads* show red blood cells in vascular structure. *Scale bars*, 100 μm for H&E. The endothelial cells were also evaluated using CD31 staining to detect blood vessels in tumors composed of 4T1-nSMase2-KD cells with or without exosome injection (*right panel*); *scale bars*, 200 μm. *E*, angiogenesis determined using CD31 staining, which was shown in *D* to detect blood vessels in tumors composed of 4T1-nSMase2-KD cells with or without exosome, as above; $n = 4$ for each group. Each *error bar* is presented as the mean ± S.E. ($n = 4$). **, $p < 0.005$, as compared with control injection.

mary epithelial cells (MCF10A); and human embryonic kidney cells (HEK293). The microarray analysis of miRNA populations in exosomes isolated from these cell lines were performed using a miRNA microarray (Fig. 4*B*). Interestingly, some of the exosomal miRNAs that were highly enriched in the metastatic cancer cell line are known to regulate angiogenesis in endothelial cells (22). One of these miRNAs, miR-210, which is well known as an angiogenic miRNA, and its expression was correlated with poor prognosis in breast cancer (23, 24). Moreover, a recent report showed that high expression levels of miR-210 in plasma are associated with the presence of tumor in patients with breast cancer and with trastuzumab resistance in patients with HER2-positive breast cancer (25). In addition, the expression level of miR-210 was significantly higher in breast cancer patients with lymph node metastasis than in breast cancer patients without lymph node metastasis (25). From our data

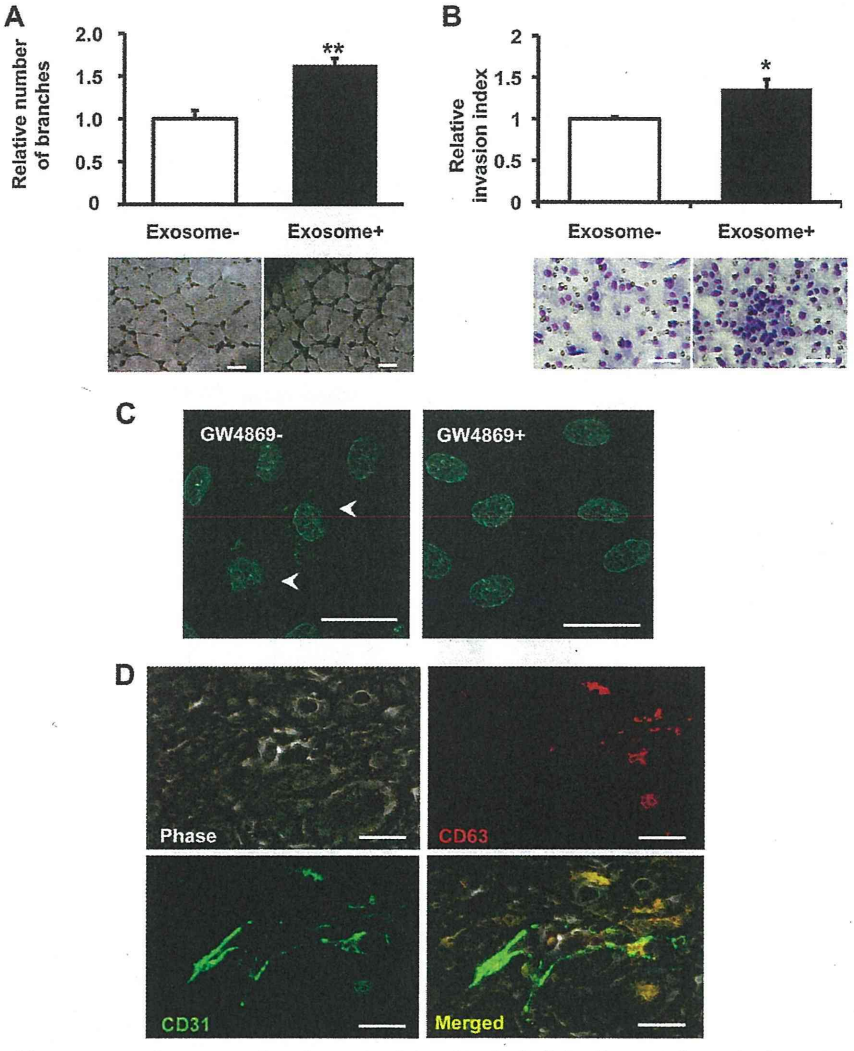


FIGURE 3. **Exosomes derived from metastatic cancer cells enhances activity of endothelial cells.** *A*, capillary tube formation in endothelial cells seeded onto Matrigel following the addition of exosomes from parental 4T1 cells. A representative image at 16 h after plating is shown, including the quantification of the average number of branches at 16 h after plating. The *scale bar* indicates 500 $\mu$m. *B*, the effect of exosome on HUVEC migration was determined by Transwell migration assay. A representative image at 48 h after plating is shown, including the quantification of the average number of migrated HUVECs at 48 h after plating. The *scale bar* indicates 100 $\mu$m. *C*, an *in vitro* co-culture system was used, whereby 4T1 cells were seeded in the *top compartment* and separated from HUVECs in the *bottom compartment* by a porous membrane. 4T1 cells (*top compartment*) were transduced with a CD63-GFP vector and co-cultured with HUVECs (*bottom compartment*). *Scale bars*, 100 $\mu$m. *D*, immunostaining of CD31 (*green*) and CD63 (*red*) on 4T1-hCD63 inoculated tumor. The *scale bar* indicates 10 $\mu$m. CD63 is co-localized with CD31-positive endothelial cells.

and previous reports, because the contribution of exosome against cancer metastasis was mediator of endothelial activation, we postulated that exosomal miR-210 might be one of the regulators in exosome for the angiogenesis around the cancer cells. Indeed, miR-210 expression in exosome was higher in malignant cancer cells than that in non-malignant cancer cell or non-cancer cells (Fig. 4*C*). To confirm that exosomal miR-210 were down-regulated in nSMase2-impaired cancer cells, we performed a qRT-PCR analysis for these cells. As shown in Fig. 4*D*, the expression of exosomal miR-210 was down-regulated in nSMase2 knockdown cells when compared with control cells, although the cellular levels of the miRNAs were not altered (supplemental Fig. 8*B*). Moreover, we performed a co-culture experiment using 4T1-nSMase-KD cells or parental 4T1 cells with HUVECs and then measured the expression of miR-210 in the HUVECs. Co-culture with parental 4T1 cells, compared with 4T1-nSMase-KD cells, led to the higher detection of miR-210 in HUVECs (Fig. 4*E*), indicating that exosomal miR-210 from metastatic cancer cells transfer to recipient endothelial cells. Then, we employed this co-culture system to study the effects of exosomes isolated from parental 4T1 cells on the expression of the established miR-210 target gene, ephrin-A3 (26). The presence of parental 4T1 cells reduced the expression level of ephrin-A3 in HUVECs compared with 4T1-nSMase2-KD cells (Fig. 4*F*). To exclude the possibility that the exosome from cancer cells itself induces the endogenous expression of miR-210 in HUVECs, we quantified the expression of primary miR-210 in HUVECs co-cultured with parental 4T1 cells or 4T1-nSMase-KD cells. As shown in supplemental Fig. 8*C*, we did not find any difference of primary miR-210